Shock-wave-like structures induced by an exothermic neutralization reaction in miscible fluids

Dmitry Bratsun,[1] Alexey Mizev,[2] Elena Mosheva,[2] and Konstantin Kostarev[2]
[1]*Department of Applied Physics, Perm National Research Polytechnical University, 614990 Perm, Russia*
[2]*Institute of Continuous Media Mechanics, 614013 Perm, Russia*
(Received 11 May 2017; revised manuscript received 1 August 2017; published 10 November 2017)

We report shock-wave-like structures that are strikingly different from previously observed fingering instabilities, which occur in a two-layer system of miscible fluids reacting by a second-order reaction $A + B \rightarrow S$ in a vertical Hele-Shaw cell. While the traditional analysis expects the occurrence of a diffusion-controlled convection, we show both experimentally and theoretically that the exothermic neutralization reaction can also trigger a wave with a perfectly planar front and nearly discontinuous change in density across the front. This wave propagates fast compared with the characteristic diffusion times and separates the motionless fluid and the area with anomalously intense convective mixing. We explain its mechanism and introduce a new dimensionless parameter, which allows to predict the appearance of such a pattern in other systems. Moreover, we show that our governing equations, taken in the inviscid limit, are formally analogous to well-known shallow-water equations and adiabatic gas flow equations. Based on this analogy, we define the critical velocity for the onset of the shock wave which is found to be in the perfect agreement with the experiments.

DOI: 10.1103/PhysRevE.96.053106

I. INTRODUCTION

In recent years, the interaction between reaction-diffusion phenomena and convective instabilities has attracted increasing interest both from the fundamental point of view and numerous applications. A second-order $A + B \rightarrow S$ reaction is distinguished among other reactions by a comparatively simple, albeit nonlinear, kinetics. If two species are initially separated in space, then this reaction can form a reaction front studied in a number of works [1,2] within a scaling theory applied to an infinite system. If the reaction occurs in a two-layer miscible system under gravity, then it may result in various buoyancy-driven instabilities which have been intensively studied both experimentally and theoretically over the past decade [3–10]. It has been found that the chemically induced changes of solution properties may provoke the instabilities in otherwise stable situations. Recently, De Wit with colleagues [11] have made a courageous attempt to classify all variety of possible convective patterns. The asymptotic theory, similar to those developed in Ref. [1], was applied to analyze the stability of large time density profiles depending on the solutal expansion and diffusion coefficients of species. It was shown that there exists one of the following instabilities or their combination. The Rayleigh-Taylor (RT) convection occurs when a denser solution is placed above a less dense one. The double diffusive (DD) instability arises if a lower component diffuses faster than an upper one and the diffusive-layer convection (DLC) develops in a case of faster upper component.

We have showed recently [10,12,13] that the classification [11] is not complete, since the effect of a concentration-dependent diffusion (CDD) was not accounted for and have reported new diffusive type of instability.

We report a pattern formation which is fundamentally different from the common fingering process. We show both experimentally and theoretically that a neutralization reaction occurring in a miscible system under gravity can also trigger a plane shock wave and explain its mechanism. We also point out a remarkable analogy between our governing equations and classical problems with shock-wave dynamics. In the paper, the term "shock wave" means a generalized wave which propagates fast, but is not necessarily supersonic, compared with characteristic velocity in a given media.

II. EXPERIMENTAL RESULTS

The experiments were performed in a vertically oriented Hele-Shaw (HS) cell made of two glass plates separated by a thin spacer of 1.2 mm (2 mm, 4 mm) thickness which assigned the inner sizes of the rectangular cavity, width 25 mm and height 90 mm. The HS cell was filled with two-layer system composed of aqueous solutions of nitric acid HNO_3 and one of bases LiOH, NaOH, or KOH. The initial concentration of reagents was varied within $(0 \div 3)$ mol/l to ensure the stable density stratification and to exclude the RT instability. During the filling of the cell with the upper solution the lower layer was separated by a thin plastic slide tightly inserted in two narrow (0.3 mm) slots made in the walls. The reagents came into contact after the plastic slide was gently taken out. Fizeau interferometry was used to visualize a refractive index distribution caused by temperature and concentration inhomogeneities. Silver-coated hollow glass spheres of neutral buoyancy were added to the liquids to observe the convective patterns. The temperature was measured by a movable thermocouple. In addition, we visualized the pH distribution by adding a small amount of universal acid-base indicator. All experiments were done at $(24 \pm 1)\,^{\circ}$C.

The analysis of the experiments made with different acid-base pairs of various initial concentrations allows us to combine all the results into two general groups which differ in convective instability scenarios. The first one is characterized by the development of a relatively weak buoyancy-driven convection caused by different diffusion mechanisms. Since the salt being produced in the reaction front diffuses more slowly than either of the reagents, the DLC or CDD instability develops in the upper layer, whereas the DD convection can arise in the lower layer. This scenario, except CDD, develops

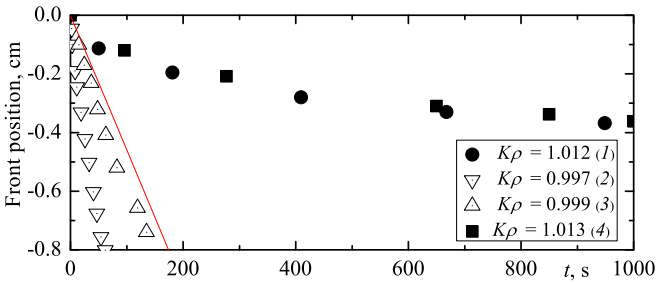

FIG. 1. Time evolution of the reaction front position obtained experimentally for different values of K_ρ. Solid line corresponds to the theoretical estimate for the critical value of the front speed (15) to trigger a shock wave.

in accordance with the instabilities classification given in Ref. [11]. This regime is characterized by both the relatively slow propagation of the reaction front (see Fig. 1, filled symbols) and small temperature excess in the reaction front which is not higher as 0.5 K. The reaction lasts a few hours to several days, depending on the initial concentration of the reagents, and its reaction rate is about 10^{-4} mol/ l s. By taking into account that the reaction rate is about of the rate of diffusion processes and that the convective instabilities are of the diffusive origin, the above scenario can be defined as a diffusion-controlled (DC) regime.

The completely different scenario not covered by the classification [11] has been observed in the second group of the experiments. Right after the solutions were brought into contact, the vigorous plumes arise above the reaction front. In only a few seconds the intense convective flow occupies the whole upper layer homogenizing the solution (Fig. 2). The flow provides continuous supply of the reagents and removal of the salt near the reaction front, which in turn enhances the flow itself due to the increase of the reaction rate. This manifests itself in much faster propagation of the reaction front (see Fig. 1, open symbols), the temperature at which can rise up to 7 K. As a result, one can observe the development of a shock-wave-like pattern (see the Supplementary Video [14]). There is an abrupt change in temperature, density, and velocity in the moving reaction front which separates the motionless fluid ahead of it and the area with intensive convective mixing behind of it. The reaction lasts from 7 to 15 min, depending on the initial concentration of the reagents, which corresponds to the reaction rate of the order of $(10^{-3} \div 10^{-2})$ mol/l s. We name this scenario as a convection-controlled (CC) regime.

In order to distinguish two regimes let us introduce a new nondimensional parameter defined as a ratio of the reaction zone density ρ_{rz} to the upper layer density ρ_{up}

$$K_\rho \equiv \frac{\rho_{rz}}{\rho_{\text{up}}} = \frac{\rho_0\left(1 + \beta_s \frac{C_{\min}}{\delta_D} + \beta_{\text{res}} \frac{C_{\max} - C_{\min}}{\delta_D}\right)}{\rho_{\text{up}}}, \qquad (1)$$

where ρ_0 is the solvent density, β is solutal expansion coefficient, C is the concentration, and subscripts s and res denote the variables related to the salt and the residual reagent taken in excess, respectively. $C_{\min}$ and $C_{\max}$ are the minimal and maximal initial concentrations in the pair of reagents, and $\delta_D = D_{\text{slow}}/D_{\text{fast}} + 1$ shows the ratio of diffusion coefficients of slow and fast reagents for a given pair of species. For better

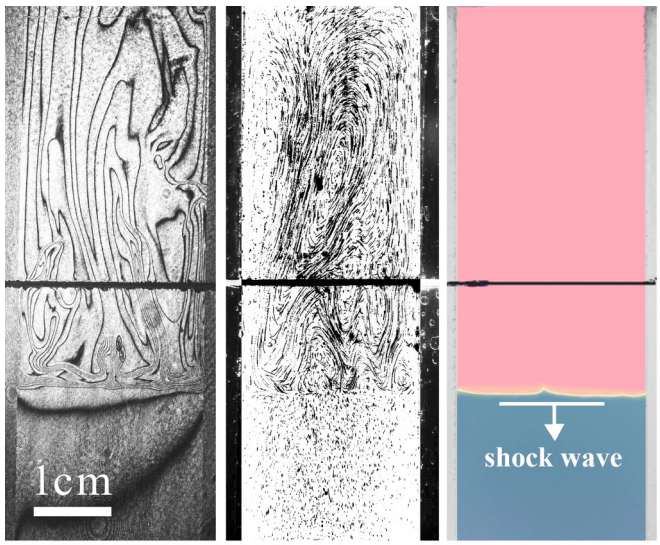

FIG. 2. Shock-wave structure observed in 150 s after the aqueous solutions of HNO_3 (upper layer) and NaOH were brought into contact. The frames from left to right correspond to interferogram showing a refractive index distribution, velocity field revealed by the traces of light-scattering particles and pH distribution obtained due to universal indicator, respectively. The initial concentrations of acid and base are equal to 1.5 mol/l and 1.4 mol/l, respectively. The initial contact line is indicated by the horizontal band. $K_\rho = 0.997$.

results, the CDD effect [10] must be taken into account in (1). The value of K_ρ uniquely defines the instability scenario. If $K_\rho < 1$, then the ρ_{rz} is smaller than ρ_{up}, which provokes the local RT instability and triggers the CC evolution in all systems (Fig. 3). When $K_\rho > 1$, the density distribution remains globally stable, making the diffusion the only mass

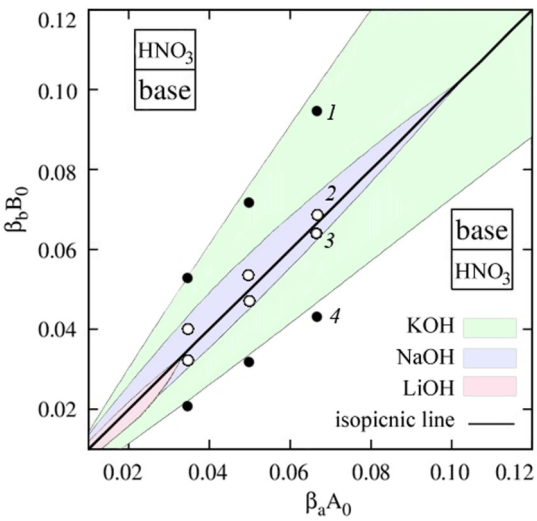

FIG. 3. Map of chemoconvection modes at the plane of the initial concentrations A_0, B_0, and expansion coefficients β_a, β_b of species. The shaded areas correspond to the shock-wave appearance at $K_\rho < 1$. The open and filled circles indicate the CC and DC regimes experimentally observed for NaOH/HNO_3, respectively. The numbered circles correspond to the experimental results shown in Fig. 1.

transfer mechanism at the initial stage. Later, the DD, DLC, or CDD instabilities can result in a weak convective motion, which, nevertheless, is not able to change significantly the reaction rate. This case corresponds to the DC regime.

The map of the DC and CC regimes is presented in Fig. 3. The isopycnic line halves the map into zones where either acid (above the line) or base (below the line) is placed in the upper layer. The shaded areas adjacent to the isopycn correspond to the CC regime ($K_\rho < 1$) for different acid-base pairs. The DC regime ($K_\rho > 1$) is realized outside this area. For better perception of the figure a few experimental points only for the pair NaOH-HNO_3 are shown in the map. These results are in perfect agreement with the calculations based on the formula (1).

III. THEORETICAL MODEL

We consider two aqueous solutions of acid A and base B filling a thermoisolated HS cell with the semigapwidth d. Right after the process starts, the reagents with initial concentrations A_0, B_0 diffuse into each other and are neutralized at the rate k with the formation of salt S and heat release Q. The system geometry is given by a two-dimension domain with x axis directed horizontally and z-axis antidirected to gravity. We scale the problem by using $2d$, $4d^2/D_{a0}$, $D_{a0}/2d$, $QA_0/\rho_0 c_p$, A_0 as the length, time, velocity, temperature, and concentration scales, respectively. D_{a0}, ν, c_p stands for acid diffusivity, kinematic viscosity and heat capacity.

The mathematical model we develop consists in the set of equations for species coupled to Navier-Stokes and energy equations, written in the dimensionless form [10]:

$$\partial_t \Phi + 1.2J(\Psi,\Phi) = \mathrm{Sc}(\nabla^2\Phi - 12\Phi - \partial_x \rho), \tag{2}$$

$$\partial_t T + J(\Psi,T) = \mathrm{Le}\nabla^2 T + \alpha AB, \tag{3}$$

$$\partial_t A + J(\Psi,A) = \nabla D_a(A)\nabla A - \alpha AB, \tag{4}$$

$$\partial_t B + J(\Psi,B) = \nabla D_b(B)\nabla B - \alpha AB, \tag{5}$$

$$\partial_t S + J(\Psi,S) = \nabla D_s(S)\nabla S + \alpha AB, \tag{6}$$

$$\rho = R_a A + R_b B + R_s S - RT, \tag{7}$$

where J stands for the Jacobian determinant $J(F,P) \equiv \partial_z F \partial_x P - \partial_x F \partial_z P$. Here we use a two-field formulation for motion equation and introduce the stream function Ψ and vorticity $\Phi = -\nabla^2\Psi$. Diffusion terms in Eqs. (4)–(6) are written to take into account the CDD effect [10]:

$$\begin{aligned} D_a(A) &\approx 0.158A + 0.881, \\ D_b(B) &\approx -0.087B + 0.594, \\ D_s(S) &\approx -0.284S + 0.478. \end{aligned} \tag{8}$$

The parameters are the Schmidt and Lewis numbers $\mathrm{Sc} = \nu/D_{a0}$, $\mathrm{Le} = \chi/D_{a0}$, the Damköhler number $\alpha = 4KA_0d^2/D_{a0}$, the set of solutal Rayleigh numbers $R_i = 8g\beta_i A_0 d^3/\nu D_{a0}$, $i = \{a,b,s\}$, and the Rayleigh number $R = 8g\beta Q A_0 d^3/\rho_0 c_p \nu D_{a0}$. Their values for the pair HNO_3/NaOH can be estimated as follows: $\mathrm{Sc} = 317$, $\mathrm{Le} = 42$, $\alpha = 10^3$, $R_a = 3.2 \times 10^5$, $R_b = 3.8 \times 10^5$, $R_s = 5.1 \times 10^5$, $R = 2.5 \times 10^4$. In the calculations, we apply a no-slip boundary condition for velocity and a zero-flux condition for all species and temperature.

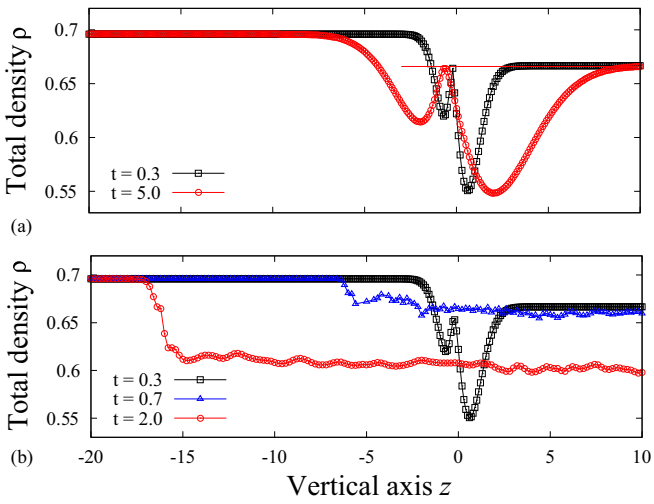

FIG. 4. Time evolution of a transverse averaged total density $\rho(z,t)$ for HNO_3/NaOH: (a) the case when the density of the reaction zone is equal to those of upper layer: $K_\rho = 1$; (b) the CC regime at $K_\rho = 0.997$ (the circle *2* in Fig. 3). In the last case, nonlinear simulations clearly shows the appearance of the shock wave for $t > 0.5$ after the collapse of the depleted zone low in density.

Figure 4 (top) shows the evolution of the density profile within a linear theory for the bifurcation case: $K_\rho = 1$. To see nonlinear development of the disturbances, the problem (2)–(7) has been solved numerically by a finite-difference method [15]. While the linear theory demonstrates slow evolution of the base state within DC dynamics, the nonlinear evolution clearly shows the formation of the shock wave at $K_\rho = 0.997$ [Fig. 4 (bottom)]. The pattern is formed as a result of the collapse of a depleted zone low in density. This implies the inapplicability of the assumption of the large time asymptote used in Ref. [11] to classify all possible solutions and indicates a much more complicated bifurcation structure. Finally, Fig. 5 demonstrates how intense mixing occurs behind the shock wave front: Almost complete mixing of salt occurs already after the expiration of one unit of time (≈317 s).

IV. ANALOGY WITH CLASSICAL SHOCK-WAVE PROBLEMS

The unexpected experimental findings has made us pay attention to the mathematical formalism of the problem. The set of classical equations governing a two-dimensional supersonic flow of an isentropic (adiabatic) compressible gas can be written as it follows [16]:

$$\frac{\partial \rho}{\partial t} + \frac{\partial \rho U}{\partial x} + \frac{\partial \rho V}{\partial y} = 0, \tag{9}$$

$$\frac{\partial U}{\partial t} + U\frac{\partial U}{\partial x} + V\frac{\partial U}{\partial y} = -\frac{C^2}{\gamma\rho}\frac{\partial \rho}{\partial x}, \tag{10}$$

$$\frac{\partial V}{\partial t} + U\frac{\partial V}{\partial x} + V\frac{\partial V}{\partial y} = 0, \tag{11}$$

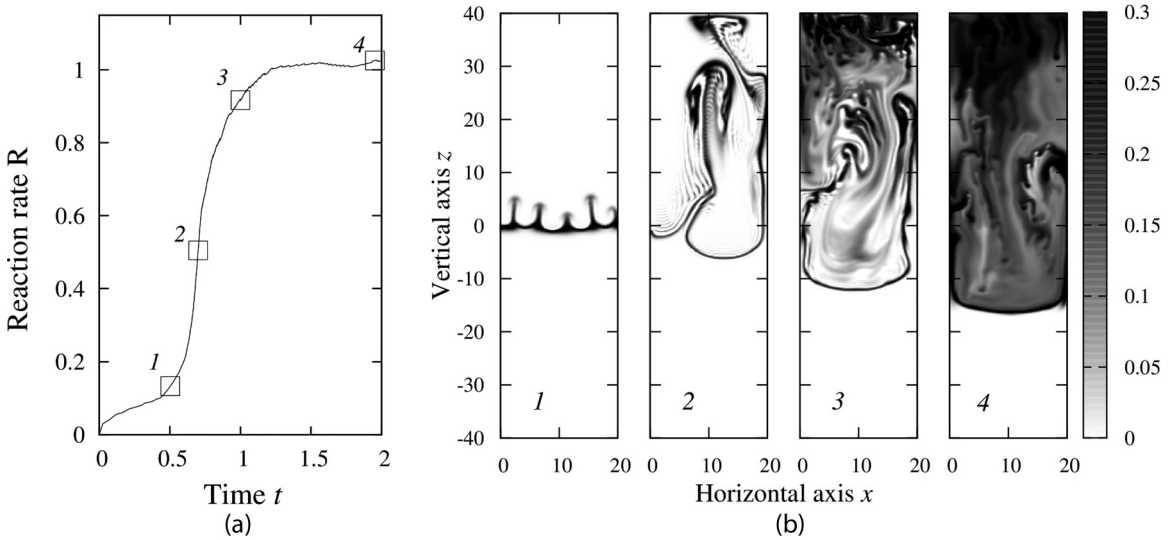

FIG. 5. (a) Time evolution of the spatial reaction rate computed as the number of points where salt $S(x,z,t)$ is larger than a given small threshold $S^* = 0.001$ normalized by the area of the domain behind the traveling shock wave; (b) the frames from left to right show the salt concentration at successive times. $K_\rho = 0.997$.

where U and V are velocity components and ρ and P stand for the density and pressure of gas, respectively. It is assumed in (9)–(11) that the main gas flow occurs in the x direction and the channel width in the y direction is much smaller. Since the flow is isentropic, we have $P\rho^\gamma = \text{const}$, where γ stands for the adiabatic index. Another important relation is given by the sound speed: $C = \sqrt{\gamma P/\rho}$.

The equations given by (9)–(11) has a remarkable mathematical analog with the equations for long gravity waves at the free surface of a shallow-water layer, which was first discussed in 1911 by Isaachsen in Ref. [17]. This analogy is the textbook example when the same equations describe two systems with completely different physics [16]. The Saint-Venant equation system [18] describing two-dimensional unsteady flows of water below a free surface in an open narrow channel with the constant bed slope within hydraulic approximation can be written as follows:

$$\frac{\partial h}{\partial t} + \frac{\partial hU}{\partial x} + \frac{\partial hV}{\partial y} = 0, \tag{12}$$

$$\frac{\partial U}{\partial t} + U\frac{\partial U}{\partial x} + V\frac{\partial U}{\partial y} = -g\frac{\partial h}{\partial x} - bU + gs, \tag{13}$$

$$\frac{\partial V}{\partial t} + U\frac{\partial V}{\partial x} + V\frac{\partial V}{\partial y} = -bV, \tag{14}$$

where h is the water depth, U and V are velocity components, g is the acceleration due to gravity, b is the viscous drag coefficient, and s is the constant bed slope taken for the definiteness along the x axis. In the inviscid limit $b = 0$ and no bed slope $s = 0$ (excluding the case of the constant bed slope, see below), the system of shallow water (12)–(14) is thus formally identical to the Eqs. (9)–(11). The velocity $C^* = \sqrt{gh}$ here plays the part of the sound velocity C in gas dynamics. If the shallow-water flow moves with velocities higher than the critical velocity C^*, one can observe the formation of the shock-wave-like structure known as "hydraulic jump" [16]. Thus, the gas compressibility is simulated here by the deformation of the free surface of an incompressible fluid. This analogy has been intensively used in theoretical physics since 1911. For example, the mechanism of a stellar core collapse was experimentally studied on the basis of the physics of hydraulic jumps [19].

One can demonstrate that a set of equations for fluid flows with dissolved reacting species in a Hele-Shaw cell under the action of gravity can be reduced either to the shallow water equations (12)–(14) and, under some additional assumptions, to the isentropic gas flow equations (9)–(11). Hele-Shaw cell is a closed parallelepiped cavity significantly compressed in one of the horizontal direction, as shown in Fig. 6: $L \gg 2d$, $H \gg 2d$. Thus, the fluid flow may be considered quasi-two-dimensional [20]. By taking into account the no-slip boundary conditions for the velocity on wide sidewalls of the cell, the variations of velocity across the gap can be approximated by the Poiseuille profiles [21]. Evolution equations in the Hele-Shaw approximation for the narrow channel $L \ll H$ then are

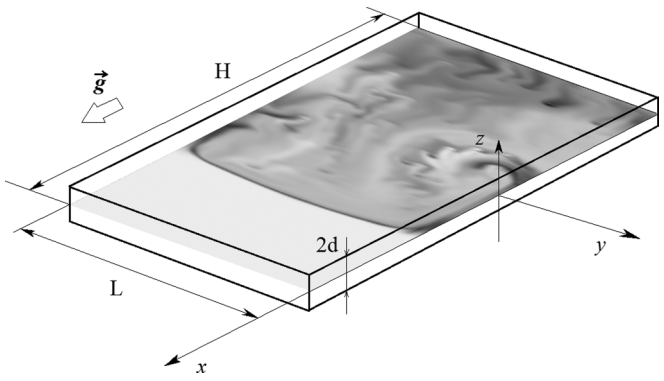

FIG. 6. Schematic presentation of a Hele-Shaw cell.

obtained by averaging the Navier-Stokes equations across the gap:

$$\frac{\partial \rho}{\partial t} + \frac{\partial \rho U}{\partial x} + \frac{\partial \rho V}{\partial y} = 0, \tag{15}$$

$$\frac{\partial U}{\partial t} + \frac{6}{5}U\frac{\partial U}{\partial x} + \frac{6}{5}V\frac{\partial U}{\partial y} = -\frac{1}{\rho}\frac{\partial p}{\partial x} - \frac{3\eta}{\rho d^2}U + g, \tag{16}$$

$$\frac{\partial V}{\partial t} + \frac{6}{5}U\frac{\partial V}{\partial x} + \frac{6}{5}V\frac{\partial V}{\partial y} = -\frac{3\eta}{\rho d^2}V, \tag{17}$$

where ρ is the density of water with reagents dissolved in it and η is the dynamic viscosity.

Since the main effect of pressure variation is due to local density variations, which in turn is due to the ongoing chemical reactions, we can assume that the pressure distribution is approximately hydrostatic and follows:

$$p(x,y,t) = gH\rho(x,y,t), \tag{18}$$

where pressure variations in height can be neglected due to high but narrow Hele-Shaw cell.

To express the medium density ρ through the concentrations of reagents dissolved in water we can apply the Boussinesq approximation

$$\rho = \rho_0(1 + \beta_A A + \beta_B B + \beta_S S), \tag{19}$$

which demands to ignore density differences except where they appear in terms multiplied by gravity g. Here ρ_0 and $\beta_{A,B,S}$ stands for the constant water density and the set of solutal expansion coefficients, respectively. The concentrations of species in (19) are defined by the set of the reaction-diffusion equations. In fact, we assume that the medium is slightly compressible bearing in mind that chemical reactions between components dissolved in water can locally change the density of the medium even though the water itself is thought to be incompressible. The kinetics of the reaction must satisfy the continuity equation (15). For example, the first-order reaction $A \rightarrow S$, which is often regarded as a rough model of the neutralization reaction, satisfies this condition. Finally, we obtain dimensionless equations:

$$\frac{\partial p}{\partial t} + \frac{\partial pU}{\partial x} + \frac{\partial pV}{\partial y} = 0, \tag{20}$$

$$\frac{\partial U}{\partial t} + \frac{6}{5}U\frac{\partial U}{\partial x} + \frac{6}{5}V\frac{\partial U}{\partial y} = -\mathrm{Sc}\frac{\partial p}{\partial x} - 12\mathrm{Sc}U + \mathrm{GaSc}^2, \tag{21}$$

$$\frac{\partial V}{\partial t} + \frac{6}{5}U\frac{\partial V}{\partial x} + \frac{6}{5}V\frac{\partial V}{\partial y} = -12\mathrm{Sc}V, \tag{22}$$

where $\mathrm{Ga} = g(2d)^3/\nu^2$ are the Galileo number.

Thus, Eqs. (20)–(22) are identical (except for the 6/5 coefficient which usually is not critical) to the Saint-Venant equation system (12)–(14), where the pressure p acts as the water depth h, and the gravity term plays a role of the constant bed slope. In the case when the drag terms and 6/5 coefficient can be neglected, the Eqs. (20)–(22) can also be reduced formally to the adiabatic gas problem (9)–(11) by making the change of variables

$$X = x - \tfrac{1}{2}\mathrm{GaSc}^2t^2, \quad Y = y, \quad T = t,$$

$$P = p, \quad \hat{U} = U - \mathrm{GaSc}^2t, \quad \hat{V} = V,$$

meaning that we go into a coordinate system that moves along the x axis with acceleration. Then the constant term in (21) disappears and we formally arrive at the following:

$$\frac{\partial P}{\partial T} + \frac{\partial P\hat{U}}{\partial X} + \frac{\partial P\hat{V}}{\partial Y} = 0, \tag{23}$$

$$\frac{\partial \hat{U}}{\partial T} + \hat{U}\frac{\partial \hat{U}}{\partial X} + \hat{V}\frac{\partial \hat{U}}{\partial Y} = -\mathrm{Sc}\frac{\partial P}{\partial X}, \tag{24}$$

$$\frac{\partial \hat{V}}{\partial T} + \hat{U}\frac{\partial \hat{V}}{\partial X} + \hat{V}\frac{\partial \hat{V}}{\partial Y} = 0, \tag{25}$$

which is identical to the Eqs. (9)–(11) for gas dynamics.

By comparing (23)–(25) with gas dynamics equations, we conclude that the critical velocity in our case is

$$C^* = \sqrt{\mathrm{Sc}}. \tag{26}$$

This means that if the density wave moves faster than $\sqrt{\mathrm{Sc}}$, then we can hypothetically observe a subsonic analog of the shock wave in gas. In the present paper, we have demonstrated experimentally that such a wave exists. Moreover, our theory, developed on the basis of classical shock wave equations, is surprisingly in excellent agreement with the experiment. This velocity estimated for our problem as $c^* \approx 17.8$ ($c^* \approx 0.056$ mm/s in dimensional units) is indicated by the solid line in Fig. 1. It is in perfect agreement with experimental data: In order to trigger a shock-wave solution, the disturbances must move faster than $\sqrt{\mathrm{Sc}}$. We observed that as soon as the wave velocity fell below this value, the wave immediately stops and was replaced by a common fingering under DC mode. One can notice that the medium is assumed to be slightly compressible since the chemical reaction between components dissolved in water can locally change the density of the medium even though the water itself is thought to be incompressible.

In conclusion, it can be emphasized that the principal role in the excitation of shock waves is played by a chemical reaction which produces significant local differences of the density and maintains these differences for a long time. Probably, the effect cannot be reproduced in nonreactive media, since any initially prepared density differences will be quickly smoothed out by diffusion.

ACKNOWLEDGMENTS

The theoretic part of the work was supported by the Russian Ministry of Science and Education (Grant No. 3.6990.2017/8.9), while Program of UD RAS (Project No. 15-10-1-16) supported the experiments.

[1] L. Gálfi and Z. Rácz, Phys. Rev. A **38**, 3151 (1988).
[2] Z. Koza and H. Taitelbaum, Phys. Rev. E **54**, R1040 (1996).
[3] L. Rongy, P. M. J. Trevelyan, and A. De Wit, Phys. Rev. Lett. **101**, 084503 (2008).

[4] A. Zalts, C. El Hasi, D. Rubio, A. Urena, and A. D'Onofrio, Phys. Rev. E **77**, 015304 (2008).
[5] C. Almarcha, P. M. J. Trevelyan, P. Grosfils, and A. De Wit, Phys. Rev. Lett. **104**, 044501 (2010).
[6] K. Tsuji and S. C. Müller, J. Phys. Chem. Lett. **3**, 977 (2012).
[7] S. H. Hejazi and J. Azaiez, J. Fluid Mech. **695**, 439 (2012).
[8] J. Carballido-Landeira, P. M. J. Trevelyan, C. Almarcha, and A. De Wit, Phys. Fluids **25**, 024107 (2013).
[9] M. C. Kim, Chem. Eng. Sci. **112**, 56 (2014).
[10] D. Bratsun, K. Kostarev, A. Mizev, and E. Mosheva, Phys. Rev. E **92**, 011003 (2015).
[11] P. M. J. Trevelyan, C. Almarcha, and A. De Wit, Phys. Rev. E **91**, 023001 (2015).
[12] D. A. Bratsun, O. S. Stepkina, K. G. Kostarev, A. I. Mizev, and E. A. Mosheva, Micrograv. Sci. Technol. **28**, 575 (2016).
[13] E. A. Aitova, D. A. Bratsun, K. G. Kostarev, A. I. Mizev, and E. A. Mosheva, J. Appl. Mech. Tech. Phys. **57**, 1226 (2016).
[14] See Supplemental Material at http://link.aps.org/supplemental/10.1103/PhysRevE.96.053106 for videos showing evolution of the system.
[15] D. A. Bratsun, Microgravity Sci. Technol. **26**, 293 (2014).
[16] L. D. Landau and E. M. Lifshitz, *Fluid Mechanics*, 2nd ed. (Pergamon Press, Oxford, 1987).
[17] I. Isaachsen, Z. Ver. Dtsch. Ing. **55**, 215 (1911).
[18] V. T. Chow, *Open-Channel Hydraulics* (McGraw–Hill, New York, 1959).
[19] T. Foglizzo, F. Masset, J. Guilet, and G. Durand, Phys. Rev. Lett. **108**, 051103 (2012).
[20] G. K. Batchelor, *An Introduction to Fluid Dynamics* (Cambridge University Press, Cambridge, 2000).
[21] D. A. Bratsun and A. De Wit, Chem. Eng. Sci. **66**, 5723 (2011).